Heliyon 10 (2024) e29169

Contents lists available at ScienceDirect

Heliyon

journal homepage: www.cell.com/heliyon

Research article

Exosomal miR-151-3p in saliva: A potential non-invasive marker for gastric cancer diagnosis and prognosis modulated by Sijunzi decoction (SJZD) in mice

Ping Yang [a,e,1], Huijun Lei [a,b,c,1], Yue Fu [a,b,c], Cheng Chen [a,b,c], Li Tang [a], Shuaishuai Xia [b,c], Yan Guo [e], Guangyu Chen [b,c], Mengzhou Xie [b,c], Jingjing Yang [f], Feng Li [d,**], Liang Li [a,b,c,*]

[a] *Department of Chinese and Western Integrative Medicine, Hunan Brain Hospital, Clinical Medical School of Hunan University of Chinese Medicine, Changsha, Hunan, 410208, China*
[b] *Provincial Key Laboratory of TCM Diagnostics, Hunan University of Chinese Medicine, Changsha, Hunan, 410208, China*
[c] *Key Laboratory of TCM Heart and Lung Syndrome Differentiation & Medicated Diet and Dietotherapy, Hunan University of Chinese Medicine, Changsha, Hunan, 410208, China*
[d] *School of Dentistry, University of California, Los Angeles, Los Angeles, CA90095, United States*
[e] *Key Laboratory of Biomedical Information Engineering of Ministry of Education, Biomedical Informatics & Genomics Center, School of Life Science and Technology, Xi'an Jiaotong University, Xi'an, Shaanxi, 710049, China*
[f] *Community Health Service Center of Dongtang Street, Yuhua District, Changsha, Hunan, 410004, China*

ARTICLE INFO

Keywords:
Gastric cancer
Exosomal miRNAs
Sijunzi decoction (SJZD)
Spleen deficiency syndrome
Exosomal miR-151-3p

ABSTRACT

Gastric cancer (GC) is one of the most prominent malignancies that originate in the epithelial cells of the gastric mucosa and is one of the main causes of cancer-related mortality worldwide. New circulating biomarkers of exosomal RNA might have great potential for non-invasive early prognosis of GC. Sijunzi Decoction (SJZD) is a typical representative formula of the method of benefiting Qi and strengthening the spleen in Traditional Chinese Medicine (TCM). However, the effects and mechanism of SJZD in treating GC remain unclear. This study looked for biomarkers of exosomal RNA for early prognosis of GC, and explored the mechanism of SJZD in treating GC. A gastric cancer model with spleen deficiency syndrome was established in nude mice, and the curative effects of SJZD were investigated. Differentially expressed miRNAs in plasma and saliva exosomes were sequenced and analyzed. Potential target genes of these miRNAs were predicted and applied for Gene Ontology (GO) and Kyoto Encyclopedia of Genes and Genomes (KEGG) signaling pathway enrichment annotation. Overlapping miRNAs in saliva and plasma samples were analyzed, and qRT-PCR was performed for verification. miR-151a-3p was selected, and qRT-PCR further determined that miR-151a-3p was downregulated in saliva and plasma exosomes from the SJZD group. The intersected miR-151a-3p target genes were predicted and enriched in the extrinsic apoptotic signaling pathways. SJZD significantly ameliorates gastric cancer with spleen deficiency syndrome in mouse models, and exosomal miRNAs, particularly miR-151-3p,

* Corresponding author. Department of Chinese and Western Integrative Medicine, Hunan Brain Hospital, Clinical Medical School of Hunan University of Chinese Medicine, Changsha, Hunan, 410208, China.
** Corresponding author.
E-mail addresses: fengli@ucla.edu (F. Li), liliang@hnucm.edu.cn (L. Li).
[1] These authors have contributed equally to this work.

https://doi.org/10.1016/j.heliyon.2024.e29169
Received 24 July 2023; Received in revised form 1 April 2024; Accepted 2 April 2024
Available online 3 April 2024

might be modulated by SJZD in plasma and saliva. The exosomal miR-151-3p in saliva may serve as a non-invasive potential marker for gastric cancer diagnosis and prognosis.

1. Introduction

Gastric cancer (GC) originates from the gastric mucosa's epithelial cells and is a leading cause of cancer-related deaths worldwide due to its rapid progression and high recurrence rate [1,2]. Early diagnosis is challenging due to non-specific symptoms [3–5]. While gastroscopy with pathological examination is the most effective screening method, its intrusiveness makes it impractical for populous countries [6,7]. Thus, exploring non-invasive diagnostic methods for early GC detection is crucial.

Exosomes are extracellular vesicles, 40–150 nm in diameter, secreted by all cell types [8–10]. Being highly heterogeneous [11] and reflecting the phenotype of their parent cells, they contain proteins, RNA, and DNA [12–14]. While their primary function remains unclear, they are believed to act as cellular waste disposal systems [15] and play roles in intercellular communication and signal transduction [14,16]. In the tumor environment, exosomes can promote carcinogenesis by influencing angiogenesis, immunity, and metastasis [17–19]. Exosomes have been detected in various bodily fluids, including blood [20,21], and elevated exosome levels have been observed in the circulation of patients with several cancers, including gastric carcinoma [22–24]. Furthermore, Baran et al. reported that the mRNA levels of melanoma antigen-1 (MAGE-1) and human epidermal growth factor receptor-2 (HER2) were dramatically elevated in plasma exosomes of patients with gastric carcinoma [25]. Thus, circulating exosomes hold promise as non-invasive biomarkers for early cancer detection and treatment. New circulating exosomal RNA biomarkers might have great potential for GC non-invasive prognosis.

Plasma exosomes, with their bilayer vesicle structure, offer enhanced stability and advantages over traditional tumor markers in tumorigenesis and metastasis [26–28]. Saliva, a diagnostic fluid secreted by various glands, contains nucleic acids, proteins, and small molecules similar to serum, reflecting body pathophysiological changes [29–31]. Salivary exosomal RNA has been used to detect oral diseases [32,33] and cancers like breast and pancreatic [29]. Notably, GAPDH mRNA from salivary exosomes was identified in lung cancer-bearing mice [34]. This suggests exosomes from distant tissues might be absorbed by salivary glands and released into saliva. Thus, salivary exosomal mRNA holds potential as a diagnostic marker for gastric cancer.

MicroRNAs (miRNAs) are a class of small noncoding RNA molecules, typically consisting of 19–25 nucleotides. They have been shown to significantly impact gene expression regulation, particularly in relation to oncogenes and tumor suppressor genes. As a result, miRNAs are increasingly being recognized as a promising molecular tool for the noninvasive diagnosis and prognosis of cancer [35]. Several miRNAs implicated in the development of GC have been discovered, and several miRNAs are now under assessment for their potential diagnostic and/or prognostic use [36]. For example, miR-21 [37], miR-27a [38], and miR-150 [39] have been reported to regulate GC cell proliferation. miR-151-3p has been implicated in several malignancies, including colorectal cancer [40], osteosarcoma [41], cholangiocarcinoma [42], head and neck cancer [43], and other malignancies, serving as tumor-suppressive or promotive miRNA. Notably, in GC, miR-151-3p derived from gastric cancer exosomes induces M2-phenotype polarization of macrophages and promotes tumor growth [44]. However, whether exosomal miR-151-3p participates in more physiological processes in GC remains unclear.

According to Traditional Chinese Medicine (TCM) theory, gastric cancer is a deficiency symptom, with phlegm coagulation, Qi stagnation, blood stagnation, and evil heat as the symptoms and spleen deficiency as the basis [45,46]. The weakness of the spleen and stomach plays a key role in the initiation and progression of gastric cancer, which exists in the precancerous disease - precancerous lesion - gastric cancer [47,48]. In TCM, spleen deficiency is one of the most prevalent fundamental symptoms, and it is also a key pathogenesis and common symptom of gastric cancer. Sijunzi Decoction (SJZD) is a typical representative formula of the method of benefiting Qi and strengthening the spleen, which has been widely used in digestive system diseases in the past generations with clinical practice experience [49,50]. To enrich the diagnostic method of spleen deficiency in gastric cancer and the efficacy and molecular mechanism of SJZD in strengthening the spleen and Qi, in this study, a model of gastric cancer with spleen deficiency in the nude mouse was established, the expression profiles of plasma exosomal RNA and salivary exosomal RNA in model mice were identified by high-throughput sequencing, applied bioinformatics and biostatistics methods to find differentially expressed miRNAs, and biomarkers with clinical application in diagnosing and treating gastric cancer were searched for. This study aims to identify biomarkers and investigate potential molecular pathways involved in the use of SJZD to treat spleen deficiency in gastric cancer.

2. Materials and methods

Ethical statement

This study was approved by the Experimental Animal Ethics Committee of Hunan University of Chinese Medicine (approval number: LL2020061501). The experiment was conducted strictly as per NIH guidelines for the Care and Use of Laboratory Animals.

2.1. Cell line and cell culture

A human gastric carcinoma cell line, NCI–N87 (CRL-5822), was procured from ATCC (Manassas, VA, USA) and cultivated in RPMI-1640 Medium (30–2001, ATCC) containing 10% Fetal Bovine Serum (FBS, 30–2020, ATCC). All cell types were cultivated at 37 °C in a

humidified atmosphere containing 5% CO_2.

2.2. Animals

99 BALB/c (nu/nu) male nude mice (4–6 weeks old, weighing 16 g–20 g) were used in this experiment. Nude mice were provided by the Experimental Animal Center of Hunan University of Traditional Chinese Medicine (license number: SYXK [Xiang] 2019～0009). All nude mice were housed in an SPF-grade barrier system, where the following experiments were performed. Mice were fed under controlled environmental conditions (22 ± 2 °C, 55 ± 10% humidity), with unrestricted access to water in separate cages.

2.3. TCM herbs and formula

SJZD was formulated with reference to the original formula of "*Taiping Huimin Hejiju Fang*" [51,52], consisting of the *Panax ginseng* C.A.Mey., *Atractylodes macrocephala* Koidz, *Poria cocos* (Schw.) Wolf., and *Glycyrrhiza uralensis* Fisch. (in the ratio of 2:2:2:1) in the doses of 12 g, 12 g, 12 g, and 6 g. All the herbs were procured from Anhui Huizhong TCM Tablets Co., Ltd. in accordance with the original formula's proportions (20021002). Experts from the College of Pharmacy at Hunan University of Chinese Medicine certified their compliance with the 2020 edition of the People's Republic of China Pharmacopeia standards. For the consistency of the TCM formulation, SJZD was extracted according to the standard method described in the pharmacopeia. The obtained liquid was concentrated by a rotary evaporator at 75 °C to make the raw drug concentration 2 g/mL; the liquid was cooled and sealed in a dry sterilized container and stored at 4 °C.

Sennae Folium decoction was derived from the leaf of *Cassia Angustifolia*. Vahl, procuring from the Bozhou Yonggang medicinal slices factory (China). Sennae Folium (500 g) was added with 5000 mL of boiling water to seal and soak for 10 min. The drugs were filtered out, and the liquid was evaporated and concentrated into 1 kg/L of liquid by rotary evaporator at 75 °C. After cooling, the decoction was sealed in a dry sterilized container and stored at 4 °C.

2.4. Quality analysis of SJZD by ultra-performance liquid chromatography-quadrupole time-of-flight mass spectrometry (UPLC-QTOF-MS)

UPLC was performed on a Waters ACQUITY UPLC system (Milford MA), consisting of a binary solvent delivery system, an auto-sampler, and a PDA detector system. An ACQUITY UPLC BEH C18 column (1.7 μm, 2.1 mm × 100 mm) was used for all analyses at 35 °C. The mobile phase was composed of 0.1% formic acid (v/v) (A) and methanol (B). The flow rate was 0.3 mL/min with 60 min of gradient elution: 0–10 min, 10-10% B; 10–40 min, 10–100% B; 40–45 min, 100-100% B; 45–47.5 min, 100-10% B; 47.5–60 min, 10-10%B. The MS analysis was performed on a Waters ACQUITY Synapt Q-TOF/MS spectrometer connected to the Waters ACQUITY UPLC system with an electrosprayionization (ESI) source in both positive and negative ionization modes. The detailed parameters were as follows: multiple ion scanning in IDA mode for each compound, scanning range *m/z* 100–1000, spray voltage 5500 and -4500 V, temperature 550 °C, collision energy 35 ± 15 eV. TOF/MS primary scanning time 100 ms, TOF/MS/MS secondary scanning time 1150 ms. The compounds were screened automatically in the TCM MS/MS Library and TMK TCM Library provided by SCIEX Company (Massachusetts, USA), followed by manual checking in order to remove the false positive signals.

2.5. Establishment of the orthotopic xenotransplantation model of gastric cancer with spleen deficiency syndrome

For spleen deficiency syndrome, 48 BALB/c (nu/nu) nude mice were given limited feeding and gavage with Sennae Folium decoction (1 mL/d for 10 days), which has a bitter-cold cathartic effect. The success of the spleen deficiency state was determined by observing the stool condition, body mass, and food and water intake [53]. Referring to the Chinese Medicine Clinical Terminology and the Clinical Research Guidelines for the Treatment of Spleen Deficiency in Chinese Medicine, the success of modeling was determined by scoring the symptoms of spleen deficiency in nude mice: 1 point for tiredness, 1 point for squinting, 1 point for bowed back, 1 point for reduced food intake, 1 point for reduced water intake, 1 point for reduced body mass, 1 point for soft stool, and 2 points for loose stool. An increase in the sum of the scores indicates an increase in symptoms, and a score of 5 or more indicates successful modeling.

Three BALB/c (nu/nu) 4-6w male nude mice were also taken, and NCI–N87 cell suspension (2×10^6) was inoculated in the axilla on the first day of the experiment to cultivate gastric cancer tissue blocks [54]. Ten days later, when the subcutaneous graft tumors had grown to around 10 mm in diameter, they were peeled off. The small tumor blocks were implanted into the stomachs of spleen-deficient mice that had been successfully bred.

2.6. Treatment of SJZD

72 BALB/c (nu/nu) male nude mice were randomly assigned into 3 groups (24 mice per group), namely control, model, and SJZD groups. Mice in the model and SJZD groups were prepared as gastric cancer models with spleen deficiency syndrome. Then, mice in the model and SJZD groups were given free ingestion of a sterile full-value pellet diet. At the same time, mice in the SJZD group were given SJZD by gavage once daily (10.92 g/kg, the dose was computed according to the drug dose conversion formula of body surface area, equivalent to the twice dose given to a 70 kg adult) for 2 weeks. SJZD was dissolved in saline before oral administration. The control and model groups were administered the same dose of normal saline for two weeks by gavage. The mental status, eye color, behavioral activity, and stool status of the nude mice in each group were observed and recorded from the 11th to the 24th day of the experiment. On the 24th day of the experiment, nude mice were anesthetized and sacrificed after saliva and plasma collection. Gastric cancer

tissues were isolated and exfoliated; tumor weight, size, and inhibition rate were measured and calculated.

2.7. Collection of saliva and plasma

Saliva was collected from nude mice for 5–10 min on the 22nd and 24th days of the experiment. Pilocarpine (0.05 mg/100 g) was injected subcutaneously between the ears of nude mice to induce saliva secretion. After collection, saliva samples were subjected to a 15-min centrifugation (2600 g, 4 °C) in a high-speed freezing centrifuge and kept at −80 °C.

Blood was obtained from the eyes on the 24th day of the experiment, and whole blood was harvested from nude mice using 5 mL of K3 EDTA anticoagulated vacuum blood collection tubes. The plasma was separated by centrifugation as soon as possible. After centrifugation, the supernatant was divided into new sterile centrifuge tubes and stored at −80 °C.

2.8. Exosomal RNA extraction and quality control

Exosomal RNAs were extracted from saliva and plasma samples with an exoRNeasy Midi/Maxi Kit (QIAGEN), and all operations were performed as stipulated by the protocol. The eluted RNA was kept at −80 °C. Agarose gel electrophoresis was carried out to analyze RNA degradation and contamination. Nanodrop was employed to determine RNA purity. Qubit® 2.0 Fluorometer (IMPLEN, CA, USA) was applied to quantify RNA concentration. The Agilent Bioanalyzer 2100 system (Agilent Technologies, CA, USA) was used to determine RNA integrity.

2.9. cDNA library construction and quality control

A Small RNA Sample Pre-kit was employed to construct the cDNA library. Adding splices at both ends of Small RNA and then reverse transcription were used to make cDNA constructs based on the Small RNA and total RNA ligated with 5′ and 3’ adapters. PAGE gel electrophoresis was employed to separate the target DNA fragments, and gel cutting was employed to recover the cDNA library. Qubit 2.0 was subsequently applied to perform initial quantification, and the library was diluted to 1 ng/ul. Subsequently, Agilent 2100 was employed to examine the insert size of the library. qRT-PCR (effective library concentration higher than 2 nM) was conducted to quantify the effective concentration of the library, thereby validating the library quality.

2.10. Sequencing

The libraries were pooled based on the effective concentration, and then the Illumina SE50 sequencing was carried out. DNA polymerase, splice primers, and four dNTPs with base-specific fluorescent labeling (one at a time) were introduced to the reaction system in the sequencing-while-synthesizing method. Unused free dNTPs and DNA polymerase were eluted after adding all four dNTPs. The fluorescence excitation buffer was then introduced, a laser was utilized to excite the fluorescence signal, the fluorescence signal was captured, and then the optical signal was converted into sequencing bases using computer analysis. Chemical reagents were ultimately applied for fluorescence quenching and removal of the dNTP 3′-OH protecting group for the next sequencing cycle.

2.11. Differentially expressed miRNA analysis

Differentially expressed miRNAs obtained from the sequencing were analyzed using the R language (Limma package). Differential miRNAs were obtained by *t*-test using the thresholds of $P < 0.01$ and $\text{Log2(FC)} > 1$.

2.12. qRT-PCR analysis

To further investigate whether SJZD regulated exosomal miRNA expression in a dose-dependent manner, 24 BALB/c (nu/nu) mice were prepared as gastric cancer models with spleen deficiency syndrome. Then, mice in the low-dose, medium-dose, and high-dose SJZD groups were given SJZD by gavage once a day (5.48 g/kg, 10.92 g/kg or 21.84 g/kg, respectively) for 2 weeks. The model groups were administered the same dose of saline by gavage for two weeks. Exosomal RNAs were extracted from saliva and plasma samples from different groups with an exoRNeasy Midi/Maxi Kit (QIAGEN). The reverse transcription of RNA to cDNA was performed by StarScript II First-strand cDNA Synthesis Mix (GenStar, China). The expression of miR-151a-3p was examined using a SYBRGreen Realtime PCR Master Mix (GenStar). The real-time thermal cycler (Jena, German) was used for qRT-PCR. U6 expression was used as an endogenous control. The primer sequence used for qRT-PCR included the following: miR-151a-3p (reverse transcription primer: 5′-GTCGTATCCAGTGCGTGTCGTGGAGTCGGCAATTGCACTGGATACGACCCTCAA-3′, forward: 5′GCGCTAGACTGAAGCTCC-3’; reverse: 5′-CAGTGCGTGTCGTGGA-3′). U6 (forward: 5′-CTCGCTTCGGCAGCACA-3′, reverse: 5′-AACGCTTCACGAATTTGCGT-3′).

2.13. Integrated target prediction of miR-151a-3p and signaling and functional enrichment annotation

The putative miR-151a-3p target genes (with score>0.95 and binding sites 3′UTR) were analyzed using MiRWalk 3.0 (http://mirwalk.umm.uni-heidelberg.de/) and miRNA-target prediction tool Targetscan7.2 (http://www.targetscan.org/vert_72/). For the obtained 22 overlapping genes, functional enrichment of Gene Ontology (GO) and Kyoto Encyclopedia of Genes and Genomes (KEGG) pathways analyses were performed using Metascape (metascape.org/gp/index.html). Metascape is a web-based portal designed to

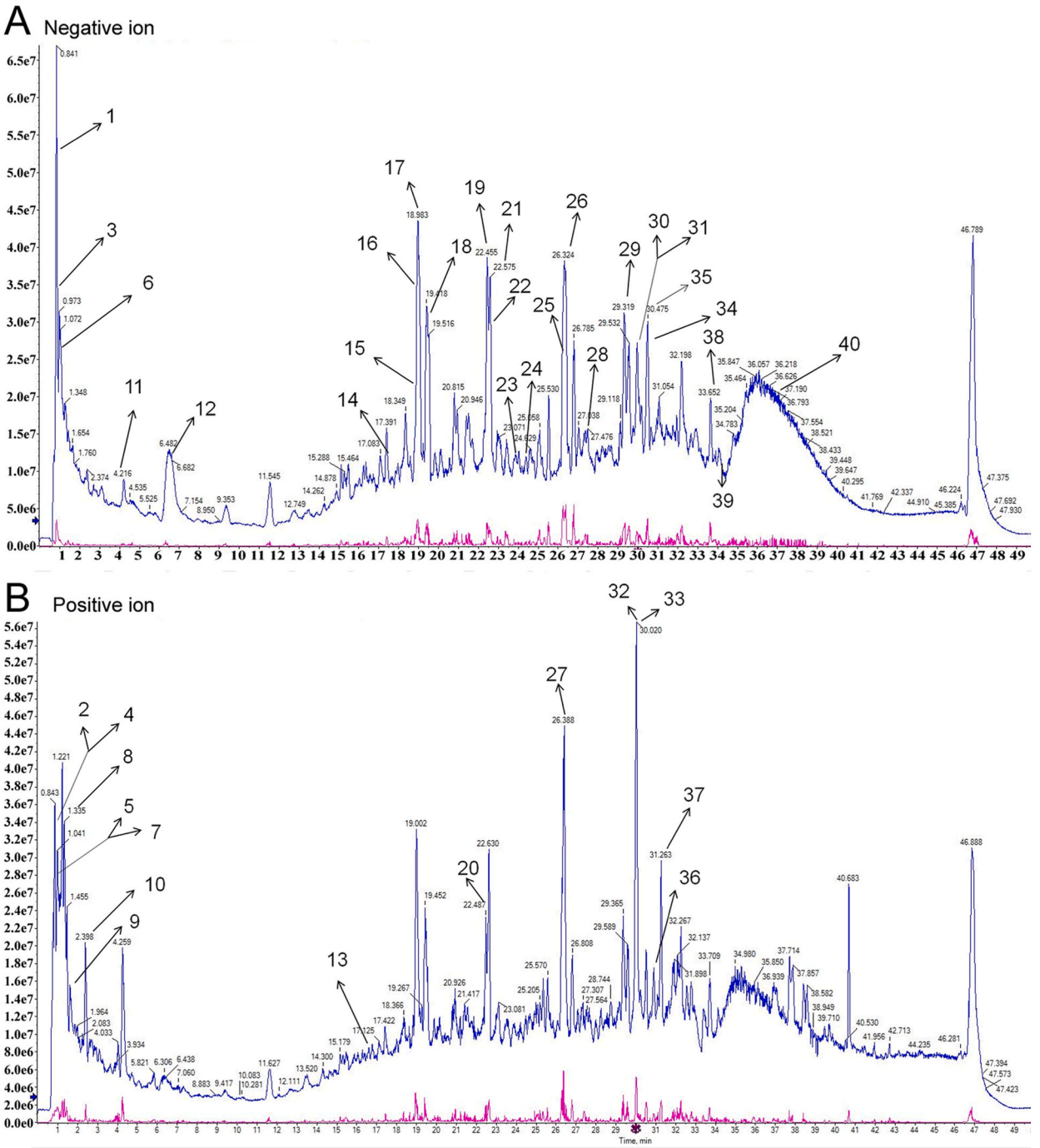

Fig. 1. The Elementary particle flow graph chromatogram in positive and negative ion mode for SJZD. (A) Negative ion Mode; (B) Positive ion Mode. The top 40 effective active components according to relative peak area are marked. 1, Quinic acid; 2, Proline; 3, L-Malic acid; 4, Adenine; 5, Pipecolinic acid; 6, Citric acid; 7, Nicotinamide; 8, Adenosine; 9, Isoleucine; 10, Phenprobamate; 11, L-Tryptophan; 12, p-hydroxyl phenylpropanol; 13, Isoscopoletin; 14, Vicenin-2; 15, Schaftoside; 16, Isoliquiritin apioside; 17, Liquiritin; 18, Liquiritin apioside; 19, Isoliquiritigenin; 20, Liquiritigenin; 21, Isoliquiritin; 22, Ononin; 23, Hydroxygenkwanin; 24, Naringenin; 25, Ginsenoside Re; 26, Ginsenoside Rg1; 27, Ganoderol B; 28, Formononetin; 29, Ginsenoside Rf; 30, Glabrene; 31, Atractylenolide III; 32, Dehydrocostus lactone; 33, Parthenolide; 34, Ginsenoside Rg2; 35, 20 (R)-Ginsenoside Rh1; 36, Germacrone; 37, Isoalantolactone; 38, Ginsenoside Rd; 39, Heterophyllin B; 40, Diammonium glycyrrhizinate.

provide a comprehensive gene list annotation and analysis resource for experimental biologists [55].

2.14. Statistical analysis

All data were presented in terms of $\bar{x} \pm s$, and data analysis was performed using SPSS 24.0 software. If the data conformed to the normal distribution and chi-square test, the comparison among groups was conducted using one-way ANOVA. Dunnett-t3 method test was used for those who did not conform to the normal distribution and chi-square test. A *P*-value of less than 0.01 was considered statistically significant.

3. Results

3.1. Quality analysis of SJZD

The main compounds of SJZD were analyzed using UPLC-QTOF-MS for validation. Totally 106 compounds were identified under negative mode, whereas 101 compounds were identified under positive mode (Supplemental Tables 1 and 2). The Elementary particle flow graph chromatogram in positive and negative ion mode for SJZD is shown in Fig. 1. Top 40 effective active components according to relative peak area were marked in Fig. 1 and Table 1.

3.2. Establishment and assessment of the spleen deficiency syndrome model in nude mice

The gastric cancer model with spleen deficiency syndrome was established as described and assessed. On days 3, 6, and 9 of the experiment, the body weight, food intake, and water consumption of nude mice in the model and SJZD groups decreased significantly

Table 1
Top 40 effective active components of SJZD according to relative peak area.

n	Retention Time	Library Hit	Molecular Mass	Negative/Positive ion	Relative Peak area(%)
1	0.83	Quinic acid	192.06294	Negative ion	0.66%
2	0.9	Proline	115.06299	Positive ion	1.37%
3	0.91	L-Malic acid	134.02021	Negative ion	1.31%
4	0.96	Adenine	135.05389	Positive ion	1.13%
5	1.11	Pipecolinic acid	129.04227	Positive ion	2.37%
6	1.14	Citric acid	192.02687	Negative ion	10.32%
7	1.14	Nicotinamide	122.04787	Positive ion	0.66%
8	1.35	Adenosine	267.0963	Positive ion	1.24%
9	1.52	Isoleucine	131.09443	Positive ion	1.15%
10	2.41	Phenprobamate	165.07875	Positive ion	2.33%
11	4.24	L-Tryptophan	204.08901	Negative ion	0.76%
12	6.53	p-hydroxyl phenylpropanol	166.06183	Negative ion	8.06%
13	16.77	Isoscopoletin	192.04188	Positive ion	0.95%
14	17.41	Vicenin-2	594.16033	Negative ion	0.45%
15	18.63	Schaftoside	564.14925	Negative ion, Positive ion	0.64%
16	18.84	Isoliquiritin apioside	550.16963	Negative ion, Positive ion	2.07%
17	18.99	Liquiritin	418.12528	Negative ion, Positive ion	13.95%
18	19.45	Liquiritin apioside	550.16804	Negative ion, Positive ion	11.29%
19	22.43	Isoliquiritigenin	256.0725	Negative ion, Positive ion	6.17%
20	22.47	Liquiritigenin	256.07261	Positive ion	6.81%
21	22.57	Isoliquiritin	418.12606	Negative ion, Positive ion	3.16%
22	22.61	Ononin	476.13246	Negative ion, Positive ion	1.64%
23	23.87	Hydroxygenkwanin	300.06319	Negative ion	0.44%
24	24.43	Naringenin	272.06766	Negative ion, Positive ion	1.10%
25	26.23	Ginsenoside Re	946.55135	Negative ion	2.82%
26	26.36	Ginsenoside Rg1	846.49815	Negative ion	5.44%
27	26.39	Ganoderol B	440.36455	Positive ion	4.12%
28	27.36	Formononetin	268.0727	Negative ion, Positive ion	3.48%
29	29.32	Ginsenoside Rf	800.49498	Negative ion	3.60%
30	29.91	Glabrene	321.11247	Negative ion	0.52%
31	29.97	Atractylenolide III	248.14078	Negative ion	0.55%
32	30.02	Dehydrocostus lactone	230.12949	Positive ion	6.52%
33	30.02	Parthenolide	248.14098	Positive ion	3.28%
34	30.07	Ginsenoside Rg2	784.50122	Negative ion	1.13%
35	30.2	20(R)-Ginsenoside Rh1	684.44603	Negative ion	0.83%
36	30.84	Germacrone	218.13143	Positive ion	0.69%
37	31.26	Isoalantolactone	232.14524	Positive ion	6.35%
38	33.65	Ginsenoside Rd	992.55758	Negative ion	1.21%
39	33.9	Heterophyllin B	778.41608	Negative ion	0.71%
40	36.81	Diammonium glycyrrhizinate	822.40564	Negative ion	6.16%

than the control group ($P < 0.01$; Fig. 2A–C). Furthermore, compared to the control group, the model construction assignment scores of nude mice in both the model and SJZD group were above 5, with significant differences ($P < 0.01$; Fig. 2D), indicating the successful construction of the spleen deficiency syndrome model.

3.3. SJZD suppresses tumor growth in gastric cancer mice with spleen deficiency syndrome

The orthotopic xenograft tumor model was established in mice with spleen deficiency syndrome, and SJZD treatment was applied (Fig. 3A). The body weight of mice in the model and SJZD groups was significantly lower than the control group ($P < 0.01$); however, SJZD treatment partially increased the body weight of model mice compared with the model group (Fig. 3B). Evaluation of tumor size and weight revealed similar evidence that, compared to the model group, SJZD therapy significantly reduced the size and weight of tumors in model mice ($P < 0.01$; Fig. 3C). These data indicate that SJZD suppresses tumor growth in gastric cancer mice with spleen deficiency syndrome.

3.4. Plasma exosomal miRNA expression in mice from different groups

Exosomal miRNAs from plasma and saliva were sequenced in order to find miRNAs with differential expression among different groups. Differentially expressed murine exosomal miRNAs in mice plasma from the control, model, and SJZD groups were displayed in hierarchical clustering heatmap and volcano plots (Fig. 4A–C). Among 507 detected murine miRNAs in the control and model groups, 87 murine miRNAs were significantly differentially expressed between the control and model groups (Fig. 4B–Table S3). Among 406 detected murine miRNAs in the model and SJZD groups, 14 murine miRNAs showing significant differential expression between the model group and the SJZD group were identified (Fig. 4C–Table S4). After sequence comparison, differentially expressed human exosomal miRNAs in mice plasma from the control, model, and SJZD groups were displayed in hierarchical clustering heatmap and volcano plots (Fig. 4D–F). Among 326 detected human miRNAs in the control and model groups, 71 human miRNAs showing significant differential expression between the control and model groups were identified (Fig. 4E–Table S5). Among 293 detected human miRNAs in the model and SJZD groups, 11 human miRNAs showing significant differential expression between the model group and the SJZD group were identified (Fig. 4F–Table S6).

Regarding the murine-derived genomic sequences, miR-128-3p (Log2(FC) = −4.346), miR-328-3p (Log2(FC) = −2.595), and miR-339-5p (Log2(FC) = −2.274) were downregulated within the model group in comparison with the control group, and their expression upregulated after SJZD treatment. miR-184-3p (Log2(FC) = 1.929), miR-1a-3p (Log2(FC) = 1.507), miR-202-5p (Log2(FC) = 2.563), miR-3470a (Log2(FC) = 3.001), miR-3470b (Log2(FC) = 3.609), miR-34c-5p (Log2(FC) = 3.015), and miR-466i-5p (Log2(FC) = 4.990) were increased within the model group in comparison with the control group, and their expression decreased after SJZD treatment.

Regarding human-derived genomic sequences, miR-128-3p (Log2(FC) = −4.418), miR-328-3p (Log2(FC) = −2.637), and miR-339-

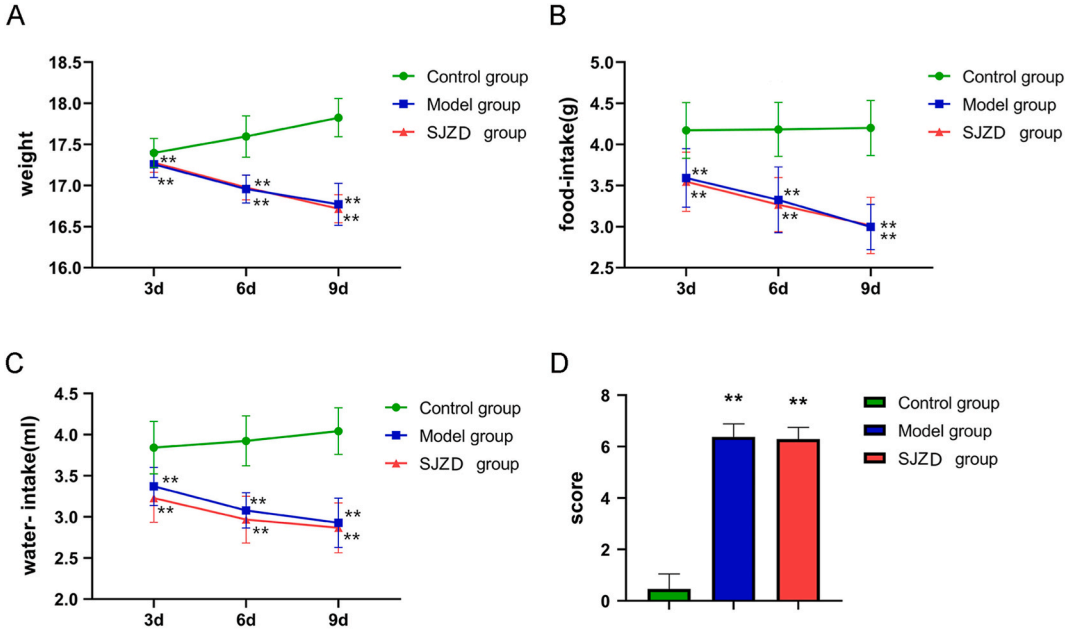

Fig. 2. Assessment of the spleen deficiency syndrome model in nude mice. (A–C) The mice's body weight, food intake, and water intake were monitored on days 3, 6, and 9 of the experiments. (D) Scoring the symptoms of spleen deficiency in nude mice.**$P < 0.01$, compared to the control group.

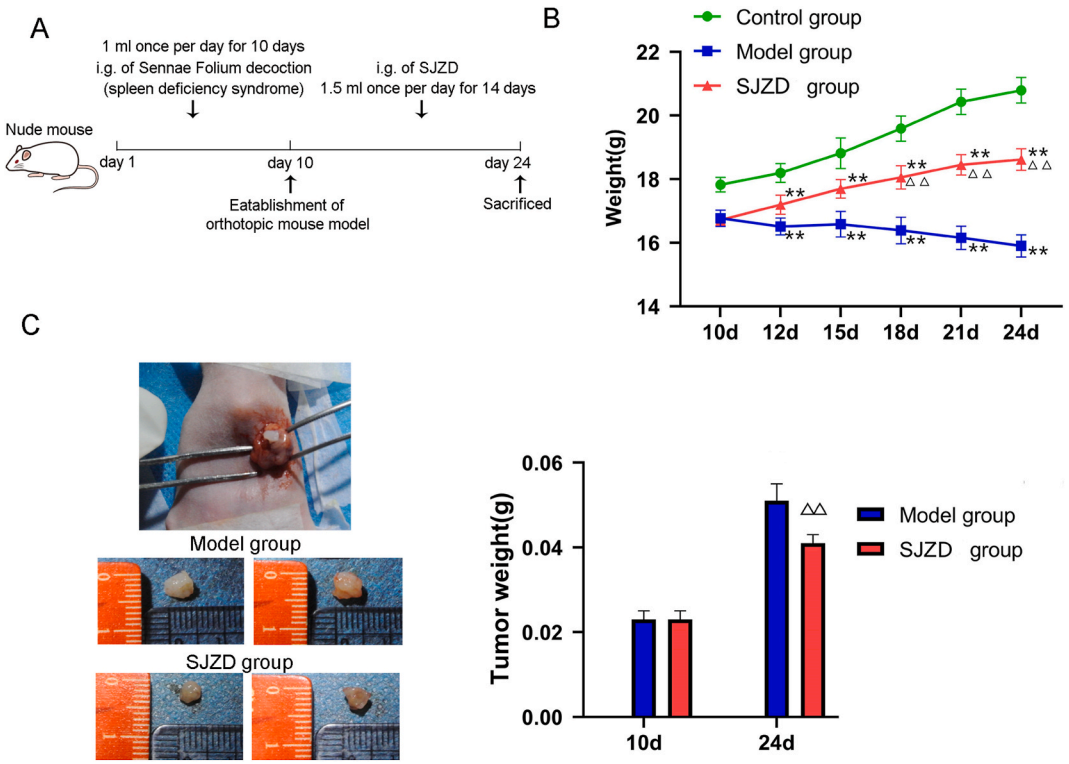

Fig. 3. Sijunzi decoction (SJZD) suppresses tumor growth in gastric cancer mice with spleen deficiency syndrome. (A) A schematic diagram showing the grouping, modeling, and treatment methods of model mice. (B) The body weight of mice in three groups was monitored on days 10, 12, 15, 18, 21, and 24 of the experiments. (C) Tumor size and weight of mice in the model and SJZD groups. n = 24. $^{**}P < 0.01$ compared with the control group; $^{\Delta\Delta}P<0.01$ compared with the model group.

5p (Log2(FC) = −2.338) were downregulated within the model group in comparison with the control group, and their expression upregulated after SJZD treatment. miR-1-3p (Log2(FC) = 1.450), miR-151a-3p (Log2(FC) = 3.267), miR-184 (Log2(FC) = 1.880), miR-202-5p (Log2(FC) = 2.511), and miR-34c-5p (Log2(FC) = 2.960) were increased within the model group in comparison with the control group, and their expression decreased after SJZD treatment.

These data suggest that SJZD might alleviate gastric cancer mice with spleen deficiency syndrome in a manner related to miR-328-3p, miR-339-5p, miR-128-3p, miR-1-3p, miR-151a-3p, miR-184, miR-202-5p, miR-34c-5p, miR-184-3p, miR-1a-3p, miR-3470a, miR-3470b, miR-466i-5p, and their target gene functions.

3.5. Functional and signaling pathway enrichment annotation of plasma exosomal miRNA targets

For further analysis of the functions and signaling pathways associated with these plasma exosomal miRNAs, TargetScan was used to predict the potential target genes of differentially expressed exosomal miRNAs in mouse plasma, and GO and KEGG enrichment annotation was then performed. Regarding biological process (BP) analysis, the main enrichment items were transcriptional positive regulation, DNA templating, transcribed DNA template, actin cytoskeleton organization, transcription from RNA polymerase II promoter, negative modulation of transcription initiation from RNA polymerase II promoter, DNA templating, phosphatidylinositol-mediated signaling, The main enrichment items were cellular junctional assembly, morphological regulation, and regulation of epithelial cell differentiation (Fig. 5A). Regarding cellular component (CC) analysis, it is mainly enriched in cell membrane, cytoplasm, cytoplasm, nucleus and other cytosolic structures, neuronal projections, Golgi membrane, synapses, presynaptic membrane, cell junctions, laminae, folds, early endosomes, endocytic vesicles, synaptic vesicles, axons and other neuronal sites, mainly for cell-matrix adhesion connections (Fig. 5A). Regarding molecular function (MF) analysis, they are mainly enriched in transcription factor activity, sequence-specific DNA binding, transcriptional coactivator activity, transcriptional activation activity, sequence-specific binding in RNA polymerase II core promoter proximal region, DNA binding in the transcriptional regulatory region, transmembrane receptor protein serine/threonine kinase activity, zinc ion binding, SMAD binding, and transcription factor binding (Fig. 5A).

KEGG pathway enrichment analysis demonstrated that it was primarily enriched in 23 signaling pathways: cholinergic synapse, melanogenesis, phosphatidylinositol signaling system, insulin secretion, MAPK signaling pathway, PI3K-Akt signaling pathway, estrogen signaling pathway, Adherens junction, colorectal cancer thyroid hormone signaling, TGF -β signaling, RAS signaling, cancer choline metabolism, Rap1 signaling, and other related pathways, prostate cancer, pancreatic cancer and other tumor signaling pathways. The aforementioned findings show differential miRNA gene expression levels in apoptosis, growth, differentiation, and

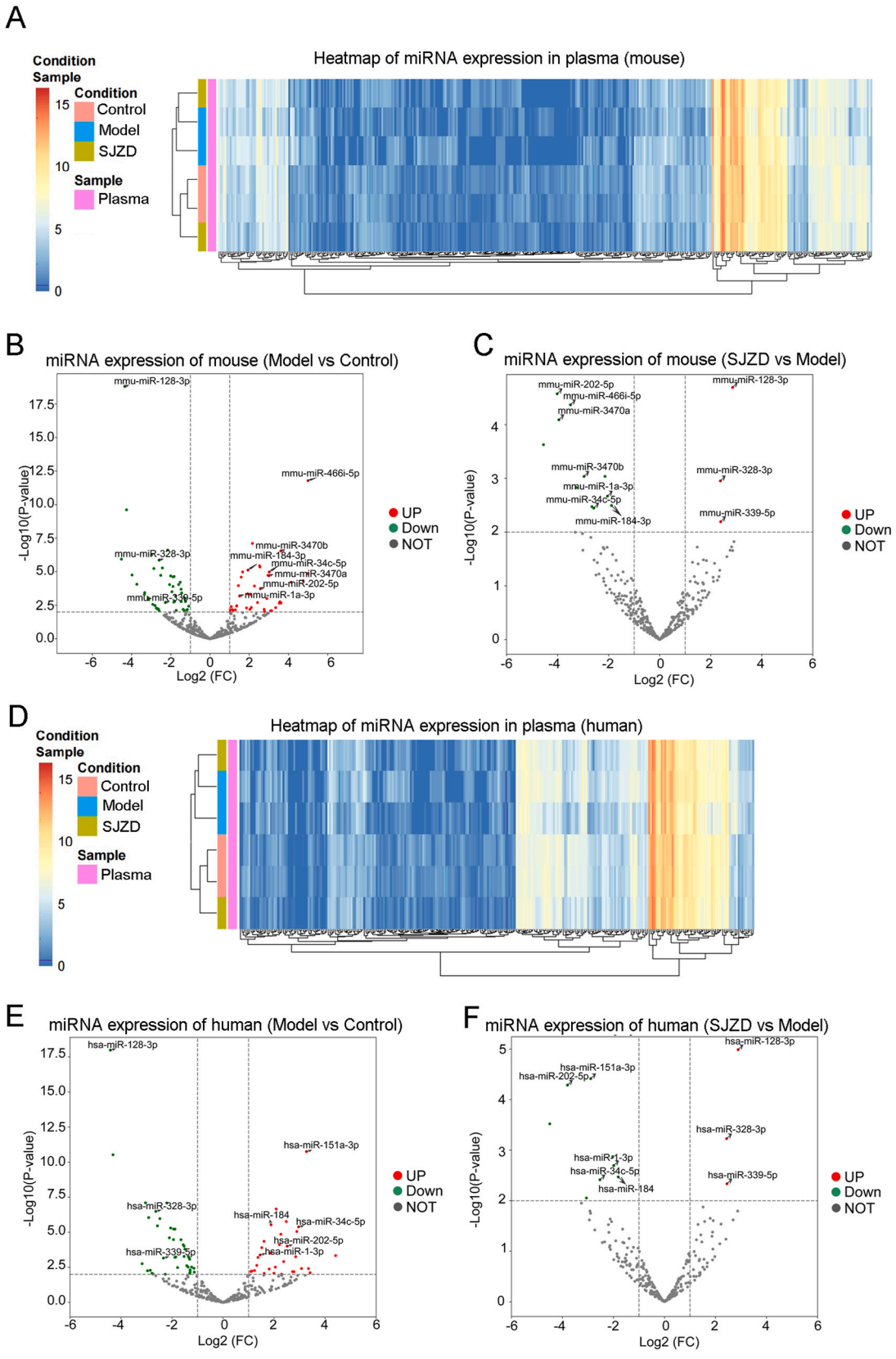

(caption on next page)

Fig. 4. Plasma exosomal miRNA expression in mice from different groups. (A–C) Hierarchical clustering heatmap and volcano plots for differentially expressed murine exosomal miRNAs in mice plasma from the control, model, and SJZD groups. (D–F) Hierarchical clustering heatmap and volcano plots for differentially expressed human exosomal miRNAs in mice plasma from the control, model, and SJZD groups.

cancer-related pathways. (Fig. 5B).

3.6. Saliva exosomal miRNA expression in mice from different groups

Next, hierarchical clustering heatmaps and volcano plots were used to reveal the differential expression of murine exosomal miRNAs in the saliva of mice from the control group, model group, and SJZD group (Fig. 6A–C). Among 274 detected murine miRNAs in the control and model groups, 7 murine miRNAs showing significant differential expression between the control and model groups were identified (Fig. 5B–Table S7). Five murine miRNAs exhibited substantial differential expression between the model and SJZD groups among the 300 detected murine miRNAs (Fig. 6C–Table S8). After sequence comparison, differentially expressed human exosomal miRNAs in mice saliva from the control, model, and SJZD groups were displayed in hierarchical clustering heatmap and volcano plots (Fig. 6D–F). Among 248 detected human miRNAs in the control and model groups, 5 human miRNAs showing significant differential expression between the control and model groups were identified (Fig. 6E–Table S9). Among 278 detected human miRNAs in the model and SJZD groups, 7 human miRNAs showing significant differential expression between the model group and the SJZD group were identified (Fig. 6F–Table S10).

Compared with the murine-derived genomic sequences, miR-184-3p (Log2(FC) = −2.377) was lower expressed within the model group in comparison with the control group, and its expression increased after SJZD treatment. Regarding human-derived genomic sequences, miR-184 (Log2(FC) = −2.129) was lower expressed within the model group in comparison with the control group, and its expression increased after SJZD treatment. miR-151a-3pexpression (Log2(FC) = 2.299) was upregulated within the model group in comparison with the control group, and its expression was downregulated after SJZD treatment. These results indicated that SJZD might exert the effect of benefiting Qi and strengthening the spleen by acting on miR-151a-3p, miR-184, and miR-184-3p.

3.7. Functional and signaling pathway enrichment annotation of saliva exosomal miRNA targets

Regarding BP analysis, the main enrichment items are RNA polymerase II promoter transcriptional positive and negative regulation, post-transcriptional RNA gene silencing, miRNA-mediated translation inhibition, glycolytic process modulation, epithelial cell migratory and apoptotic modulation, cellular response to insulin stimulation, etc. (Fig. 7A). Regarding CC analysis, the targets are mainly enriched in the nucleus, cytoplasm, cytoplasmic mRNA processing body, and extra-nucleoplasmic region (Fig. 7A). Regarding MF analysis, it is mainly enriched in transcription factor binding, zinc ion binding, ATP binding, transcriptional activation activity, sequence-specific binding of RNA polymerase II core promoter proximal region, sequence-specific binding of RNA polymerase II transcriptional regulatory region, insulin binding, etc. binding, insulin binding, etc. (Fig. 7A).

KEGG pathway enrichment analysis demonstrated that it was primarily enriched in 12 signaling pathways: central carbon metabolism, insulin signaling, HIF-1 signaling, neurotrophin signaling, renal cell carcinoma, Rap1 signaling, Foxo signaling, cancer choline metabolism, and cGMP-PKG in cancer (Fig. 7B). These analyses suggest the target genes of miRNAs are enriched in pathways associated with the regulation of apoptosis, growth, and differentiation, as well as tumor-related pathways.

3.8. Selection of promising prognostic miRNA markers for gastric cancer with spleen deficiency syndrome

For identifying potential prognostic miRNA markers for gastric cancer with spleen deficiency syndrome, overlapping miRNAs in saliva and plasma samples between the model and SJZD groups were analyzed, and hsa-miR-151a-3p and hsa-miR-184 were found (Fig. 8A). According to the sequencing results, the hsa-miR-151a-3p level decreased both in plasma and salivary exosomes after SZJD therapy. While the hsa-miR-184 level exhibited an inconsistent trend in plasma and salivary exosomes (decreased in plasma exosomes and increased in salivary exosomes). Therefore, miR-151a-3p was selected for further validation in SJZD therapy groups with varying doses. The expression levels of hsa-miR-151a-3p were examined in mice saliva and plasma samples from the model, low-dose, medium-dose, and high-dose SJZD groups using qRT-PCR. Fig. 8B shows that miR-151a-3p was downregulated in both plasma and salivary exosomes in a dose-dependent manner. Next, according to TCGA-STAD and gastric cancer-related miRNA expression microarray GSE93415, miR-151a-3p was upregulated in cancer tissues than control group samples (Fig. 8C–E). The target genes of miR-151a-3p were subsequently predicted using MirWalk 3.0 and TargetScan, and the intersection was taken (Fig. 8F). Extrinsic apoptotic signaling pathways were identified by applying functional and signaling pathway enrichment annotation in Metascope to the intersecting target genes of miR-151a-3p.(Fig. 8G). Therefore, exosomal miR-151a-3p might be an underlying biomarker in gastric cancer.

4. Discussion

In this study, a gastric cancer model with spleen deficiency syndrome was established in nude mice, and the curative effects of SJZD were investigated. Differentially expressed miRNAs in plasma and saliva exosomes were sequenced and analyzed. Potential target genes of these miRNAs were predicted and applied for GO and KEGG signaling pathway enrichment annotation. Overlapping miRNAs in saliva and plasma samples were analyzed, and miR-151a-3p was selected; intersected miR-151a-3p target genes were predicted and

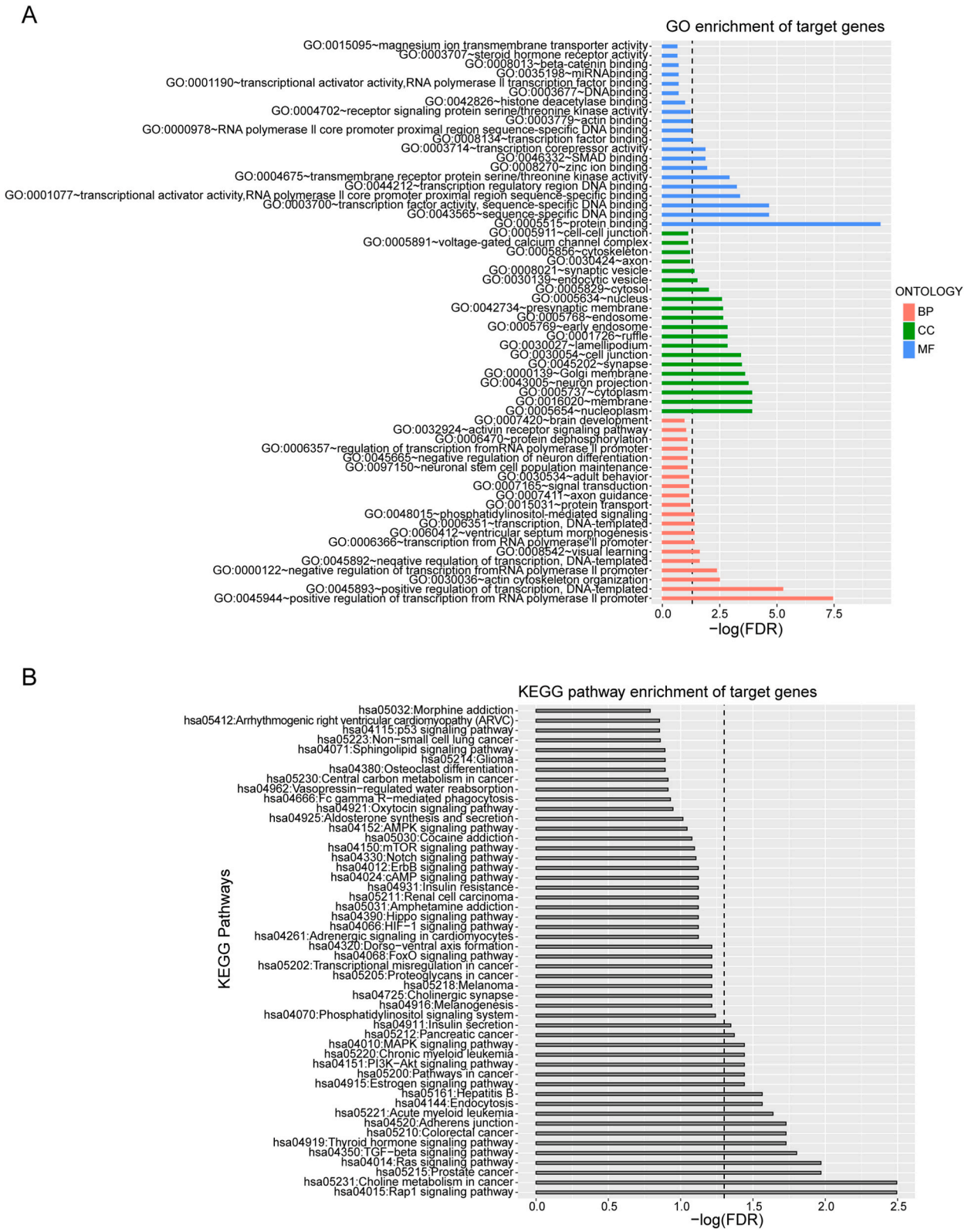

Fig. 5. Possible target genes of differentially expressed exosomal miRNAs in mice plasma were predicted by TargetScan and applied for GO functional enrichment analysis (A) and KEGG signaling pathway enrichment annotation (B).

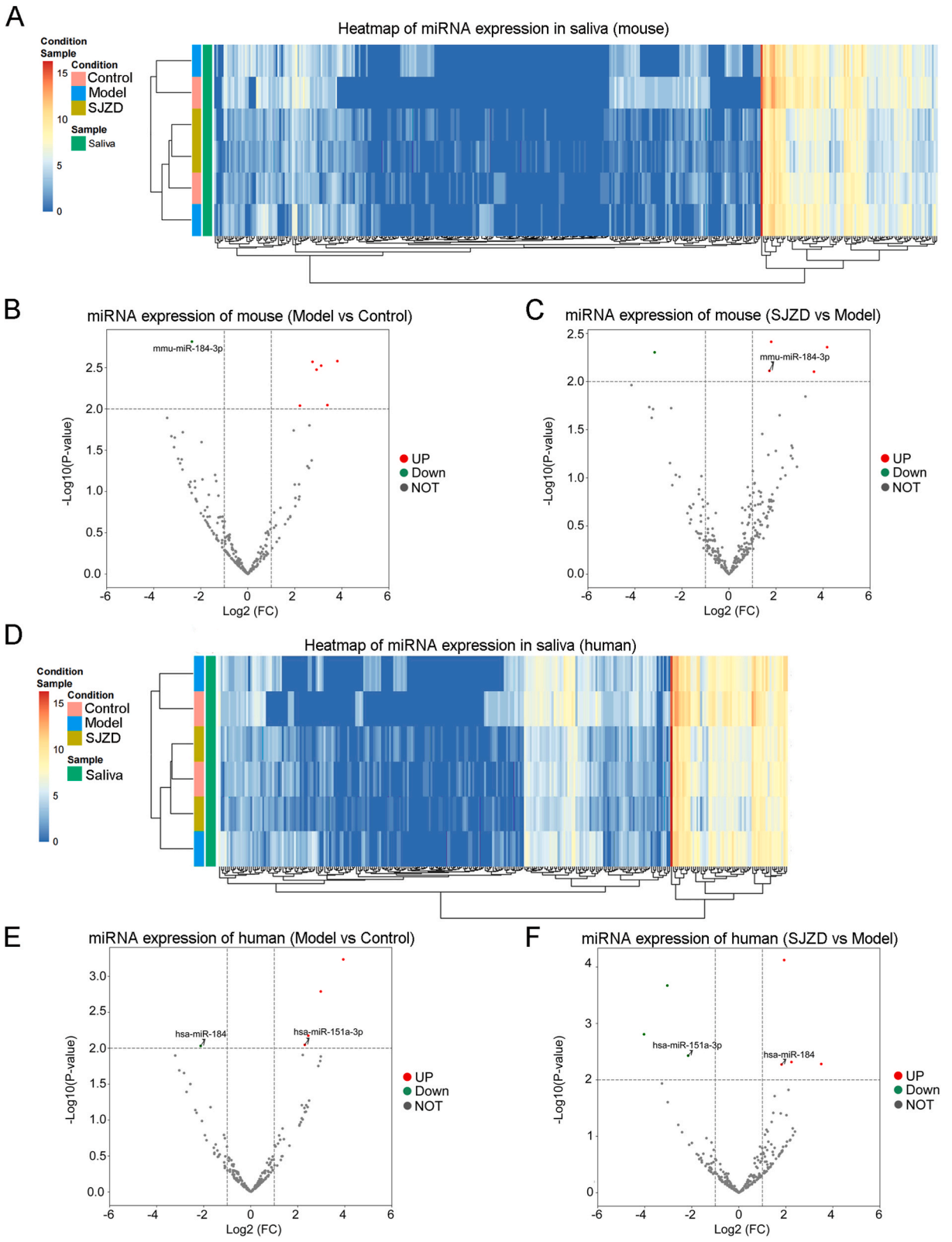

Fig. 6. Saliva exosomal miRNA expression in mice from different groups. (A–C) Hierarchical clustering heatmap and volcano plots for differentially expressed murine exosomal miRNAs in mice saliva from the control, model, and SJZD groups. (D–F) Hierarchical clustering heatmap and volcano plots for differentially expressed human exosomal miRNAs in mice saliva from the control, model, and SJZD groups.

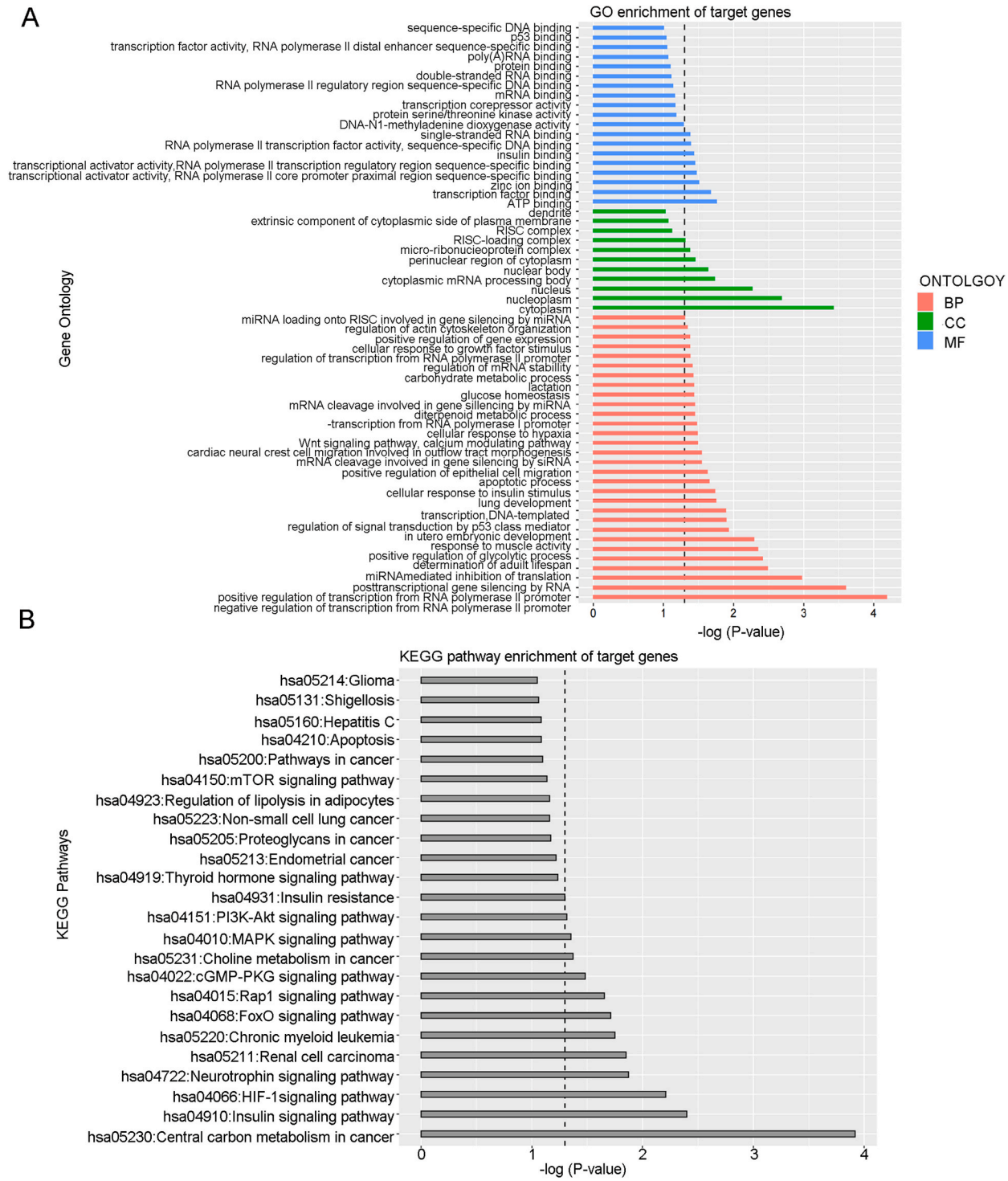

Fig. 7. Possible target genes of differentially expressed exosomal miRNAs in mice saliva were predicted by TargetScan and applied for GO functional enrichment analysis (A) and KEGG signaling pathway enrichment annotation (B).

enriched in the extrinsic apoptotic signaling pathways.

The common clinical TCM syndromes of gastric cancer include Qi deficiency and blood stagnation, liver Qi affecting the stomach, phlegm and dampness blocking the stomach, stomach heat injuring Yin, spleen and stomach deficiency, stomach Yin deficiency, and Qi and blood deficiency [56]. Jiang et al. [57] investigated 500 patients with gastric cancer and found that spleen deficiency syndrome

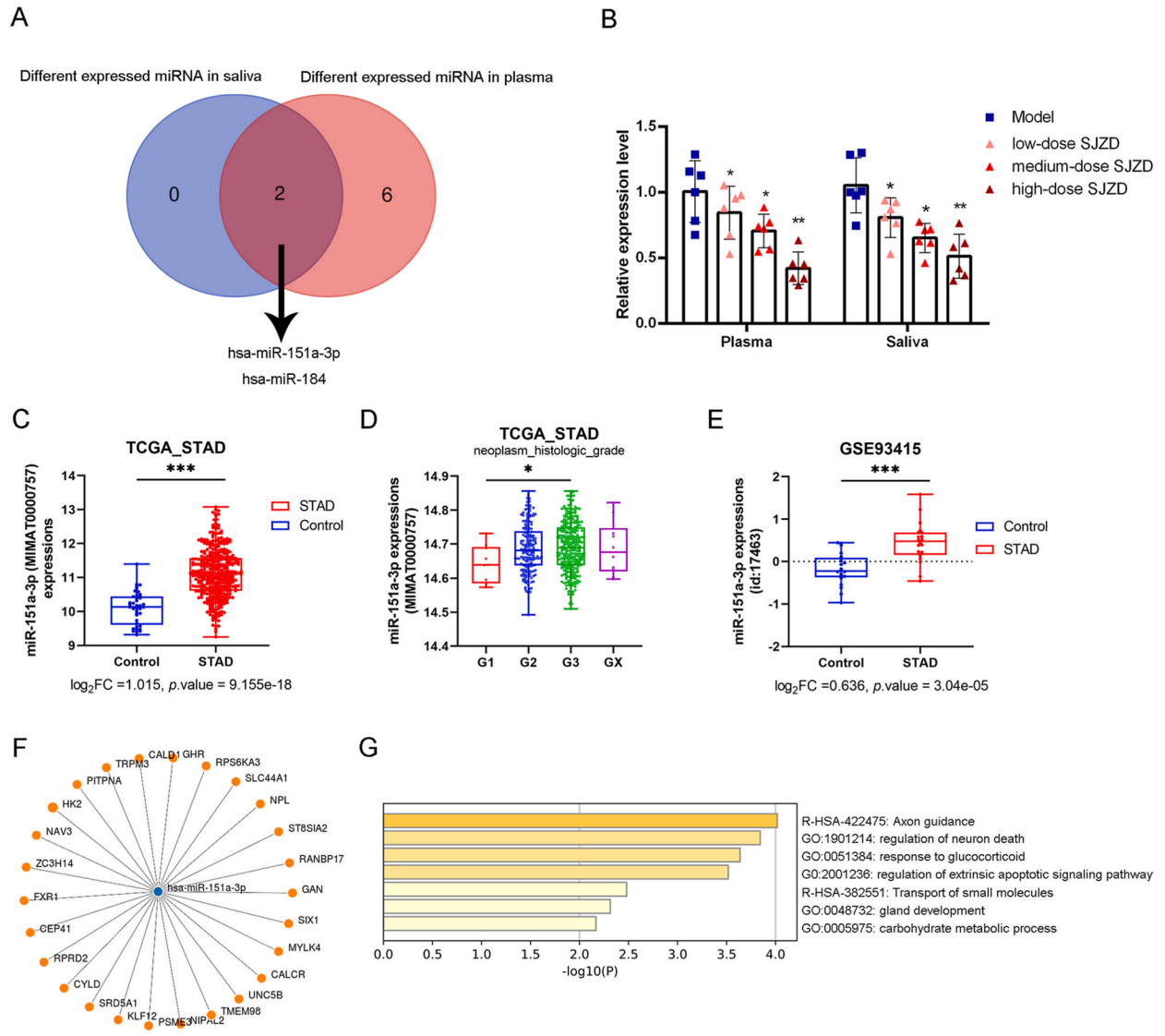

Fig. 8. Selection of promising prognostic miRNA markers for gastric cancer with spleen deficiency syndrome. (A) Overlapping miRNAs in saliva and plasma samples between the model and SJZD groups were analyzed, and hsa-miR-151a-3p and hsa-miR-184 were found. (B) The expression levels of hsa-miR-151a-3p were examined in mice saliva and plasma samples from the model, low-dose (5.48 g/kg), medium-dose (10.92 g/kg), and high-dose (21.84 g/kg) of SJZD groups using qRT-PCR. The expression levels of miR-151a-3p in control and stomach adenocarcinoma (STAD) samples according to TCGA-STAD (C–D) and GSE93415 (E). (F) Norwalk 3.0 and TargetScan were used to predict the target genes of miR-151a-3p, and the intersection was taken. (G) The intersected target genes of miR-151a-3p were applied for functional and signaling pathway enrichment annotation in Metascope. $^{*}P < 0.05$, $^{**}P < 0.01$ compared with the model group or control.

accounted for the largest proportion of the preoperative single-factor syndromes. Zhao et al. [58] divided 102 gastric cancer patients into two groups according to TCM identification criteria: gastric cancer without and with spleen deficiency syndrome, and showed that gastric cancer patients with the syndrome of spleen deficiency had a poorer clinical prognosis compared with those without spleen deficiency. In this study, in the Sennae Folium decoction-induced spleen deficiency syndrome model in nude mice, weight loss, reduced food and water intake, and tiredness and curling up were observed in the nude mice, and the symptoms were similar to those recorded in medical practice.

SJZD, which originated from the third volume of the Song Dynasty's *Taiping Huimin Hejiju Fang*, is a typical representative formula of the method of benefiting Qi and strengthening the spleen. It was found to act mainly by regulating gastrointestinal functions and enhancing the body's immunity, with anti-tumor and metabolic effects [59,60]. Tian et al. [61] found that SJZD could restore the CaM/CaMK II signaling pathway to basic normal levels in mice with spleen deficiency syndrome. Some studies have also reported the restorative effects of polysaccharides and nonpolysaccharides from SJZD on intestinal microorganisms in a model of spleen deficiency [50]. In addition, SJZD can also promote the repair of gastrointestinal mucosal damage [62]. In this study, SJZD treatment effectively

suppressed tumor growth in mice with spleen deficiency syndrome and gastric cancer, giving experimental support for the use of SJZD in the treatment of spleen deficiency syndrome and gastric cancer. Among compounds identified in this study, several have been reported to serve as anti-tumor active ingredients against GC. For example, vicenin-2 inhibits *Helicobacterium pylori* infection associated gastric carcinogensis *in vitro* via modulating Akt and Nrf2 signaling [63]. Liquiritin [64] and isoliquiritin effectively suppress proliferation and promote ROS accumulation and apoptosis of GC cell lines [65]. Ginsenoside Re, Ginsenoside Rd and Ginsenoside Rh1 have been reported to exert anti-tumor effects in GC by inhibiting GC metastasis [66] and induce GC cell apoptosis [67,68]. SJZD might exert its functions through these active ingredients, which needs to be investigated in future studies.

Numerous studies have demonstrated that exosomal microRNAs can influence a variety of cancer-related characteristics, including cancer's onset, progression, and metastasis, garnering significant attention for exosomal microRNAs [69,70], and additional evidence has indicated that exosomal miRNAs are excellent candidates as biomarkers in the era of precision medicine [71,72]. It was shown that the differential expression of serum exosomes miR-19b-3p and miR-106a-5p in gastric cancer patients correlated with lymph node metastasis and the TNM stage of gastric cancer [73]. Serum exosomal miR-423-5p showed to be more differentially expressed than CEA and CA-199 and could be used to diagnose gastric cancer [74]. In addition to plasma, as a component of human bodily fluids, saliva is affected by pathophysiological changes in the body due to variations in its constituent content [75]. In this experiment, plasma and saliva exosomal miRNAs from mice with gastric cancer and spleen deficiency syndrome were detected using high-throughput sequencing techniques, and differential exosomal miRNAs were screened by comparing gene libraries derived from humans and mice. Interaction of saliva and plasma human-derived differential miRNAs revealed that 2 human-specific differential miRNAs in plasma samples, miR-151a-3p, and miR-184, were also present in salivary exosomes. The presence of human-derived miRNAs in the saliva of nude mice, which could only originate from transplanted human cancer cell-derived tumors, suggests that changes in miRNAs in saliva can directly reflect molecular changes in gastric tumor cells, providing direct evidence for non-invasive early diagnosis of gastric cancer with spleen deficiency syndrome using saliva diagnosis.

In addition, differential salivary miRNA expression analysis revealed that miR-184 expression was lower in the model group compared to the control group when human genomic sequences were compared, and increased following SJZD treatment. miR-151a-3p was highly expressed within the model group than the control group and showed to be downregulated following SJZD treatment. miR-151a-3p showed consistent changes in expression in saliva and plasma samples, while miR-184 was inconsistently expressed in saliva and plasma samples. hsa-miR-151a-3p has been previously reported to be upregulated in the serum exosomes from gastric cancer patients [76]. Small extracellular vesicles from gastric cancer that are high in miR-151a-3p promote liver metastasis by generating a niche that increases hepatic stemness [77]. Furthermore, other studies also indicated the upregulation of circulating miR-151a-3p in esophageal adenocarcinoma [78] and cervical cancer [79] patients. Moreover, the intersected target genes of miR-151a-3p were applied for functional and signaling pathway enrichment annotation, and extrinsic apoptotic signaling pathways were found. Although the specific functions of miR-151-3p on SJZD for treating gastric cancer in patients with spleen deficiency syndrome remain unknown, targeting tumor genes with miR-151a-3p will be an important area of future research. Regarding the potential mechanisms, miR-151-5p has been reported to target p53 mRNA and down-regulate p53 levels in SC-M1 gastric cancer cells. The Notch1/miR-151-5p axis contributed to the progression of SC-M1 cells through down-regulation of p53 which in turn repressed FAK promoter activity [80]. Another study found that miR-151-3p induces M2-phenotype polarization in macrophages and increases gastric cancer tumor growth [44]. Therefore, underlying mechanisms might be multifaceted. Notably, several active components of SJZD have been reported to alter miRNA expression in GC and other diseases. Isoliquiritin ameliorates depression in mouse models via upregulating miR-27a levels [81]. Ginsenoside Rg1 administration increased miR-152 to reduce hepatic stellate cell activation [82]. Formonoetin plays an anti-GC function by regulating miR-542-5p [83]. Integrative analyses involving these compounds are necessary.

5. Conclusions

In a mouse model with spleen deficiency syndrome, SJZD significantly alleviates gastric cancer. Furthermore, exosomal miRNAs in plasma and saliva, especially miR-151-3p, might be modulated by SJZD. The presence of exosomal miR-151-3p in saliva has the potential to serve as a noninvasive diagnostic and prognostic biomarker for gastric cancer.

6. Limitation

There were some limitations in the present study. Firstly, a positive control for gastric cancer therapy, such as 5-FU and cisplatin, was not included in the treatment. A positive control could have offered a clearer baseline for evaluating the effects of SJZD interventions. Secondly, we have identified 207 compounds of SJZD extracts. However, the bioavailability and functions of compounds from SJZD extracts require further investigation.

Ethics statement

This study was approved by the Experimental Animal Ethics Committee of Hunan University of Chinese Medicine (approval number: LL2020061501).

Funding

This study was supported by grants from the National Natural Science Foundation of China (No. 82374323), the Natural Science

Foundation of Hunan Province (No. 2022JJ30435, 2019JJ40221), and the Key Research and Development Program of Hunan Province (No. 2022SK2124, 2022SK2163).

Data availability statement

The authors confirm that the data supporting the findings of this study are available within the article and supplementary materials.

CRediT authorship contribution statement

Ping Yang: Validation, Investigation, Funding acquisition, Data curation. **Huijun Lei:** Investigation. **Yue Fu:** Investigation. **Cheng Chen:** Investigation. **Li Tang:** Investigation. **Shuaishuai Xia:** Writing – original draft, Investigation. **Yan Guo:** Validation, Software. **Guangyu Chen:** Investigation. **Mengzhou Xie:** Validation, Software. **Jingjing Yang:** Writing – review & editing, Validation. **Feng Li:** Writing – review & editing, Validation, Project administration, Conceptualization. **Liang Li:** Writing – review & editing, Supervision, Funding acquisition, Conceptualization.

Declaration of competing interest

The authors declare that they have no known competing financial interests or personal relationships that could have appeared to influence the work reported in this paper.

Acknowledgments

We are grateful for the support from the Institute of Diagnostics of TCM, Hunan University of Chinese Medicine, Changsha, China.

Appendix A. Supplementary data

Supplementary data to this article can be found online at https://doi.org/10.1016/j.heliyon.2024.e29169.

References

[1] E.C. Smyth, et al., Gastric cancer, Lancet 396 (10251) (2020) 635–648.
[2] L.H. Eusebi, et al., Gastric cancer prevention strategies: a global perspective, J. Gastroenterol. Hepatol. 35 (9) (2020) 1495–1502.
[3] L. Necula, et al., Recent advances in gastric cancer early diagnosis, World J. Gastroenterol. 25 (17) (2019) 2029–2044.
[4] V. Pasechnikov, et al., Gastric cancer: prevention, screening and early diagnosis, World J. Gastroenterol. 20 (38) (2014) 13842–13862.
[5] P. Karimi, et al., Gastric cancer: descriptive epidemiology, risk factors, screening, and prevention, Cancer Epidemiol. Biomarkers Prev. 23 (5) (2014) 700–713.
[6] W. Chen, et al., Cancer statistics in China, 2015, CA A Cancer J. Clin. 66 (2) (2016) 115–132.
[7] M. Kato, Diagnosis and therapies for gastric non-invasive neoplasia, World J. Gastroenterol. 21 (44) (2015) 12513–12518.
[8] C. Kahlert, R. Kalluri, Exosomes in tumor microenvironment influence cancer progression and metastasis, J. Mol. Med. (Berl.) 91 (4) (2013) 431–437.
[9] C. Thery, L. Zitvogel, S. Amigorena, Exosomes: composition, biogenesis and function, Nat. Rev. Immunol. 2 (8) (2002) 569–579.
[10] G. Raposo, W. Stoorvogel, Extracellular vesicles: exosomes, microvesicles, and friends, J. Cell Biol. 200 (4) (2013) 373–383.
[11] J. Kowal, et al., Proteomic comparison defines novel markers to characterize heterogeneous populations of extracellular vesicle subtypes, Proc. Natl. Acad. Sci. U. S. A. 113 (8) (2016) E968–E977.
[12] C. Kahlert, et al., Identification of double-stranded genomic DNA spanning all chromosomes with mutated KRAS and p53 DNA in the serum exosomes of patients with pancreatic cancer, J. Biol. Chem. 289 (7) (2014) 3869–3875.
[13] L. Balaj, et al., Tumour microvesicles contain retrotransposon elements and amplified oncogene sequences, Nat. Commun. 2 (2011) 180.
[14] H. Valadi, et al., Exosome-mediated transfer of mRNAs and microRNAs is a novel mechanism of genetic exchange between cells, Nat. Cell Biol. 9 (6) (2007) 654–659.
[15] M. Vidal, Exosomes: revisiting their role as "garbage bags", Traffic 20 (11) (2019) 815–828.
[16] J. De Toro, et al., Emerging roles of exosomes in normal and pathological conditions: new insights for diagnosis and therapeutic applications, Front. Immunol. 6 (2015) 203.
[17] S.A. Melo, et al., Cancer exosomes perform cell-independent microRNA biogenesis and promote tumorigenesis, Cancer Cell 26 (5) (2014) 707–721.
[18] B. Costa-Silva, et al., Pancreatic cancer exosomes initiate pre-metastatic niche formation in the liver, Nat. Cell Biol. 17 (6) (2015) 816–826.
[19] H. Peinado, et al., Melanoma exosomes educate bone marrow progenitor cells toward a pro-metastatic phenotype through MET, Nat. Med. 18 (6) (2012) 883–891.
[20] S. Keller, et al., Body fluid derived exosomes as a novel template for clinical diagnostics, J. Transl. Med. 9 (2011) 86.
[21] C. Lasser, Identification and analysis of circulating exosomal microRNA in human body fluids, Methods Mol. Biol. 1024 (2013) 109–128.
[22] L. Giannopoulou, et al., Liquid biopsy in ovarian cancer: the potential of circulating miRNAs and exosomes, Transl. Res. 205 (2019) 77–91.
[23] S. Lakshmi, T.A. Hughes, S. Priya, Exosomes and exosomal RNAs in breast cancer: a status update, Eur. J. Cancer 144 (2021) 252–268.
[24] M. Mendt, et al., Generation and testing of clinical-grade exosomes for pancreatic cancer, JCI Insight 3 (8) (2018).
[25] J. Baran, et al., Circulating tumour-derived microvesicles in plasma of gastric cancer patients, Cancer Immunol. Immunother. 59 (6) (2010) 841–850.
[26] W. Zhang, X. Ou, X. Wu, Proteomics profiling of plasma exosomes in epithelial ovarian cancer: a potential role in the coagulation cascade, diagnosis and prognosis, Int. J. Oncol. 54 (5) (2019) 1719–1733.
[27] J. Wang, et al., Plasma exosomes as novel biomarker for the early diagnosis of gastric cancer, Cancer Biomarkers 21 (4) (2018) 805–812.
[28] H. Li, et al., Unique microRNA signals in plasma exosomes from pregnancies complicated by preeclampsia, Hypertension 75 (3) (2020) 762–771.
[29] C.Z. Zhang, et al., Saliva in the diagnosis of diseases, Int. J. Oral Sci. 8 (3) (2016) 133–137.
[30] M. Wozniak, C. Paluszkiewicz, W.M. Kwiatek, Saliva as a non-invasive material for early diagnosis, Acta Biochim. Pol. 66 (4) (2019) 383–388.
[31] X. Zheng, et al., Smart biosensors and intelligent devices for salivary biomarker detection, TrAC, Trends Anal. Chem. 140 (2021) 116281.

[32] P. Panta, V.R. Venna, Salivary RNA signatures in oral cancer detection, Anal. Cell Pathol. 2014 (2014) 450629.
[33] X. Xing, et al., Emerging role of exosomes in craniofacial and dental applications, Theranostics 10 (19) (2020) 8648.
[34] J. Yang, et al., Detection of tumor cell-specific mRNA and protein in exosome-like microvesicles from blood and saliva, PLoS One 9 (11) (2014) e110641.
[35] S. Filipow, L. Laczmanski, Blood circulating miRNAs as cancer biomarkers for diagnosis and surgical treatment response, Front. Genet. 10 (2019) 169.
[36] V.Y. Shin, K.M. Chu, MiRNA as potential biomarkers and therapeutic targets for gastric cancer, World J. Gastroenterol. 20 (30) (2014) 10432–10439.
[37] K. Motoyama, et al., Clinicopathological and prognostic significance of PDCD4 and microRNA-21 in human gastric cancer, Int. J. Oncol. 36 (5) (2010) 1089–1095.
[38] T. Liu, et al., MicroRNA-27a functions as an oncogene in gastric adenocarcinoma by targeting prohibitin, Cancer Lett. 273 (2) (2009) 233–242.
[39] Q. Wu, et al., MiR-150 promotes gastric cancer proliferation by negatively regulating the pro-apoptotic gene EGR2, Biochem. Biophys. Res. Commun. 392 (3) (2010) 340–345.
[40] C. Yue, et al., miR-151-3p inhibits proliferation and invasion of colon cancer cell by targeting close homolog of L1, J. Biomed. Nanotechnol. 16 (6) (2020) 876–884.
[41] X. Li, et al., Circular RNA hsa_circ_0000073 contributes to osteosarcoma cell proliferation, migration, invasion and methotrexate resistance by sponging miR-145-5p and miR-151-3p and upregulating NRAS, Aging (Albany NY) 12 (14) (2020) 14157–14173.
[42] M.E. McNally, et al., Concomitant dysregulation of microRNAs miR-151-3p and miR-126 correlates with improved survival in resected cholangiocarcinoma, HPB (Oxford) 15 (4) (2013) 260–264.
[43] R. Pastorino, et al., Plasma miR-151-3p as a candidate diagnostic biomarker for head and neck cancer: a cross-sectional study within the INHANCE consortium, Cancer Epidemiol. Biomarkers Prev. 31 (12) (2022) 2237–2243.
[44] S. Xie, et al., [miR-151-3p derived from gastric cancer exosomes induces M2-phenotype polarization of macrophages and promotes tumor growth, Xi Bao Yu Fen Zi Mian Yi Xue Za Zhi 38 (7) (2022) 584–589.
[45] W. Xu, et al., Traditional Chinese medicine for precancerous lesions of gastric cancer: a review, Biomed. Pharmacother. 146 (2022) 112542.
[46] L. Zhang, et al., Systems pharmacology to reveal multi-scale mechanisms of traditional Chinese medicine for gastric cancer, Sci. Rep. 11 (1) (2021) 22149.
[47] L.R. Fu, S.W. Guo, X.H. Liu, Effect of Yiqi Jianpi plus anticancer herbs on spleen deficiency in colorectal cancer and its anti-tumor role, Asian Pac. J. Tropical Med. 7 (5) (2014) 378–381.
[48] L. Yang, et al., Traditional Chinese medical comprehensive therapy for cancer-related fatigue, Chin. J. Integr. Med. 22 (1) (2016) 67–72.
[49] D. Gan, et al., Chinese classical formula sijunzi decoction and chronic atrophic gastritis: evidence for treatment approach? Evid Based Complement Alternat Med 2017 (2017) 9012929.
[50] P. Ma, et al., Differential effect of polysaccharide and nonpolysaccharide components in Sijunzi decoction on spleen deficiency syndrome and their mechanisms, Phytomedicine 93 (2021) 153790.
[51] K. An, et al., Simultaneous quantification of ten active components in traditional Chinese formula sijunzi decoction using a UPLC-PDA method, J Anal Methods Chem 2014 (2014) 570359.
[52] Y. Liu, J. Yang, Z. Cai, Chemical investigation on Sijunzi decoction and its two major herbs Panax ginseng and Glycyrrhiza uralensis by LC/MS/MS, J. Pharm. Biomed. Anal. 41 (5) (2006) 1642–1647.
[53] W.L. Zhang, et al., Establishment of a mouse model of cancer cachexia with spleen deficiency syndrome and the effects of atractylenolide I, Acta Pharmacol. Sin. 41 (2) (2020) 237–248.
[54] G. Zhang, et al., The building of orthotopic transplanted model of gastric tumor in 615 mice with OB anastomotic glue pasted method, Journal of Zhejiang Chinese Medical University 37 (5) (2013) 587–590.
[55] Y. Zhou, et al., Metascape provides a biologist-oriented resource for the analysis of systems-level datasets, Nat. Commun. 10 (1) (2019) 1523.
[56] X. Qian, K. Xu, Clinical study on the relationship between TCM syndromes and prognostic factors in gastric cancer, Jilin Journal of Chinese Medicine 32 (11) (2012) 1088–1091.
[57] C. Jiang, S.-Y. Lin, J.-L. Zhao, Retrospective study on the dynamic development of Chinese medical syndrome types of gastric cancer, Chin. J. Integrated Tradit. West Med. 33 (1) (2013) 44–46.
[58] Q. Zhao, et al., Relationship between splenic deficiency syndrome and biological behavior in patients with gastric carcinoma: the clinical curative effects of shenqifuzheng injection, Journal of Beijing University of Traditional Chinese Medicine 26 (4) (2003) 68–71.
[59] X. Chen, et al., Meta-analysis of efficacy of sijunzi decoction combined with enteral nutrition for the treatment of gastric cancer, Nutr. Cancer 72 (5) (2020) 723–733.
[60] J. Jia, et al., Sijunzi decoction-treated rat serum induces apoptosis of side population cells in gastric carcinoma, Exp. Ther. Med. 15 (2) (2018) 1718–1727.
[61] R. Tian, et al., Study on interference effect of Sijunzi decoction on brain-gut CaM/CaMK II of spleen Qi deficiency syndrome rats, China J. Chin. Mater. Med. 40 (20) (2015) 4075–4079.
[62] Y. Lu, et al., Sijunzi Decoction attenuates 2, 4, 6-trinitrobenzene sulfonic acid (TNBS)-induced colitis in rats and ameliorates TNBS-induced claudin-2 damage via NF-κB pathway in Caco2 cells, BMC Compl. Alternative Med. 17 (1) (2017) 35.
[63] Y. Zhang, et al., Vicenin-2 inhibits the Helicobacterium pylori infection associated gastric carcinogenic events through modulation of PI3K/AKT and Nrf2 signaling in GES-1 cells, J. Biochem. Mol. Toxicol. 35 (3) (2021) e22680.
[64] R. Xie, et al., Combining TRAIL and liquiritin exerts synergistic effects against human gastric cancer cells and xenograft in nude mice through potentiating apoptosis and ROS generation, Biomed. Pharmacother. 93 (2017) 948–960.
[65] M. Yu, et al., Isoliquiritigenin inhibits gastric cancer growth through suppressing GLUT4 mediated glucose uptake and inducing PDHK1/PGC-1α mediated energy metabolic collapse, Phytomedicine 121 (2023) 155045.
[66] Z. Yang, et al., Ginsenoside Rh1 regulates gastric cancer cell biological behaviours and transplanted tumour growth in nude mice via the TGF-β/Smad pathway, Clin. Exp. Pharmacol. Physiol. 49 (12) (2022) 1270–1280.
[67] B.J. Kim, Involvement of melastatin type transient receptor potential 7 channels in ginsenoside Rd-induced apoptosis in gastric and breast cancer cells, J. Ginseng. Res. 37 (2) (2013) 201–209.
[68] H.J. Jang, et al., Anticarcinogenic effects of products of heat-processed ginsenoside Re, a major constituent of ginseng berry, on human gastric cancer cells, J. Agric. Food Chem. 62 (13) (2014) 2830–2836.
[69] C.G. Lengyel, et al., The emerging role of liquid biopsy in gastric cancer, J. Clin. Med. 10 (10) (2021).
[70] Z. Wang, et al., The miR-223-3p/MAP1B axis aggravates TGF-β-induced proliferation and migration of BPH-1 cells, Cell. Signal. 84 (2021) 110004.
[71] Y.R. Lee, et al., Circulating exosomal noncoding RNAs as prognostic biomarkers in human hepatocellular carcinoma, Int. J. Cancer 144 (6) (2019) 1444–1452.
[72] S. Kim, et al., Serum exosomal miRNA-145 and miRNA-200c as promising biomarkers for preoperative diagnosis of ovarian carcinomas, J. Cancer 10 (9) (2019) 1958–1967.
[73] L. Zhao, et al., The role of exosomes and "exosomal shuttle microRNA" in tumorigenesis and drug resistance, Cancer Lett. 356 (2 Pt B) (2015) 339–346.
[74] H. Yang, et al., Exosomal miR-423-5p targets SUFU to promote cancer growth and metastasis and serves as a novel marker for gastric cancer, Mol. Carcinog. 57 (9) (2018) 1223–1236.
[75] M.A.R. Buzalaf, et al., Saliva as a diagnostic tool for dental caries, periodontal disease and cancer: is there a need for more biomarkers? Expert Rev. Mol. Diagn 20 (5) (2020) 543–555.
[76] X. Qian, et al., Identification of key circulating exosomal microRNAs in gastric cancer, Front. Oncol. 11 (2021) 693360.
[77] B. Li, et al., miR-151a-3p-rich small extracellular vesicles derived from gastric cancer accelerate liver metastasis via initiating a hepatic stemness-enhancing niche, Oncogene 40 (43) (2021) 6180–6194.
[78] L. Jamali, et al., Circulating microRNAs as diagnostic and therapeutic biomarkers in gastric and esophageal cancers, J. Cell. Physiol. 233 (11) (2018) 8538–8550.
[79] G. Ma, et al., Circulating plasma microRNA signature for the diagnosis of cervical cancer, Cancer Biomarkers 26 (4) (2019) 491–500.

[80] K.W. Hsu, et al., Notch1 pathway-mediated microRNA-151-5p promotes gastric cancer progression, Oncotarget 7 (25) (2016) 38036–38051.
[81] Y. Li, et al., Isoliquiritin ameliorates depression by suppressing NLRP3-mediated pyroptosis via miRNA-27a/SYK/NF-κB axis, J. Neuroinflammation 18 (1) (2021) 1.
[82] R. Zhang, et al., Ginsenoside Rg1 epigenetically modulates Smad7 expression in liver fibrosis via MicroRNA-152, J. Ginseng. Res. 47 (4) (2023) 534–542.
[83] W.-S. Wang, C.-S. Zhao, Formononetin exhibits anticancer activity in gastric carcinoma cell and regulating miR-542-5p, Kaohsiung J. Med. Sci. 37 (3) (2021) 215–225.